MINERALOGICAL MAGAZINE, MARCH 1985, VOL. 49, PP. 49–58

Calcium-poor pyroxenes: phase relations in the system $CaO–MgO–Al_2O_3–SiO_2$

G. M. BIGGAR

Department of Geology, University of Edinburgh, West Mains Road, Edinburgh EH9 3JW

ABSTRACT. Using previously published data and a few new data the compositions of protopyroxene, orthopyroxene, and pigeonite, coexisting with liquid in the system $CaO–MgO–SiO_2$, are reviewed and shown to depend subtly on the number and nature of the coexisting phases such as forsterite, silica, other pyroxene, and liquid. Broadly, protopyroxene contains 0 to 1.0 wt. % CaO, orthopyroxene 1.4 to 2.2%, and pigeonite 3.0 to 6.5%, but pigeonite coexisting with olivine contains up to 1.5 wt. % more CaO than pigeonite coexisting with SiO_2 at the same temperature.

In the system $CaO–MgO–Al_2O_3–SiO_2$ some new analyses and all previously published microprobe analyses of pyroxenes fall into three compositional groups, which are hereafter used to name the pyroxene irrespective of whatever description the original authors gave to their products. For these groups, the compositional subtleties depend on the number and nature of coexisting phases and these are illustrated using sketches of the solid solution polyhedron for each phase, to illustrate, in particular, the decomposition of pigeonite as temperature drops, at 1276 °C when forsterite, diopside and liquid coexist, but at other temperatures when other phases coexist. The assemblage orthopyroxene, anorthite, diopside, forsterite is established as the solidus at 1244 °C by X-ray diffraction and by new microprobe analyses, and not protopyroxene with anorthite, diopside, and forsterite as was previously accepted. Liquidus surfaces for forsterite and protopyroxene, forsterite and orthopyroxene, and forsterite and pigeonite, are drawn, with temperature data, and several crystallization paths demonstrate the double resorption boundaries, forsterite–protopyroxene–orthopyroxene–liquid and forsterite–orthopyroxene–pigeonite–liquid, and demonstrate crystallization of four pyroxenes, resorption of three of them, and reprecipitation of a second generation of one of them.

No new data are presented for the solidus of the system $CaO–MgO–SiO_2$, but a reinterpretation of the existing data suggests that the solvi of these alumina-free pyroxenes do not show an increase in CaO as temperature decreases. This is contrary to previous interpretations which have mingled data for alumina-bearing and alumina-free pyroxenes. The reinterpretation also favours the reaction protoenstatite + pigeonite $\rightleftharpoons$ orthopyroxene at 1375 °C and a revision of the previously accepted *P–T* (Schreinemaker's) net for the pyroxenes is proposed which does *not* accept orthopyroxene $\rightleftharpoons$ protopyroxene + diopside at 1100 °C at one bar, which previously has always been accepted by extrapolation from the experimental data at 1 kbar.

KEYWORDS: Ca-poor pyroxenes, phase relations, system $CaO–MgO–Al_2O_3–SiO_2$.

IN the system $CaO–MgO–SiO_2$ the data and discussion by Longhi and Boudreau (1980) are an outstanding example of careful work, observation, and elucidation of previous errors and misconception, but an even greater understanding of crystalline pyroxene compositions can be obtained from their data. The data are replotted in figs. 1 to 3 along with some other previous data and a few new data (Table I).

The liquidus fields of orthopyroxene and pigeonite, based on the data of Longhi and Boudreau, are shown in fig. 1 with some data from Kushiro (1972) all as presented by Longhi and Boudreau except that temperature contours have been added. Some of the same liquidus data points are shown in fig. 2 but with the CaO contents of the coexisting *solid* phase (pigeonite) shown and contours of the CaO content of the solid pigeonite are suggested. CaO increases as temperature decreases. The CaO contours (fig. 2) are at an angle to the temperature contours (fig. 1) such that pigeonite in equilibrium with olivine at a given temperature contains about 1.5 wt. % more CaO than pigeonite in equilibrium with tridymite (see also fig. 5).

Detail of the crystalline compositions is better seen in fig. 3 which shows for pigeonite a difference in the SiO_2 content, as well as in the CaO content, for pigeonite at a given temperature, depending on the phase it is in equilibrium with, as described in the caption to fig. 3.

Longhi and Boudreau comment on metastability. Pigeonite at 1380 °C in equilibium with diopside in a one week run retains more CaO than in the three runs at 1378 °C for one month; orthopyroxene compositions shown as plus signs at 1400 °C were interpreted as metastable, despite run lengths of 143 hours. Such orthopyroxene compositions were not found in runs of 304 and 451 hours.

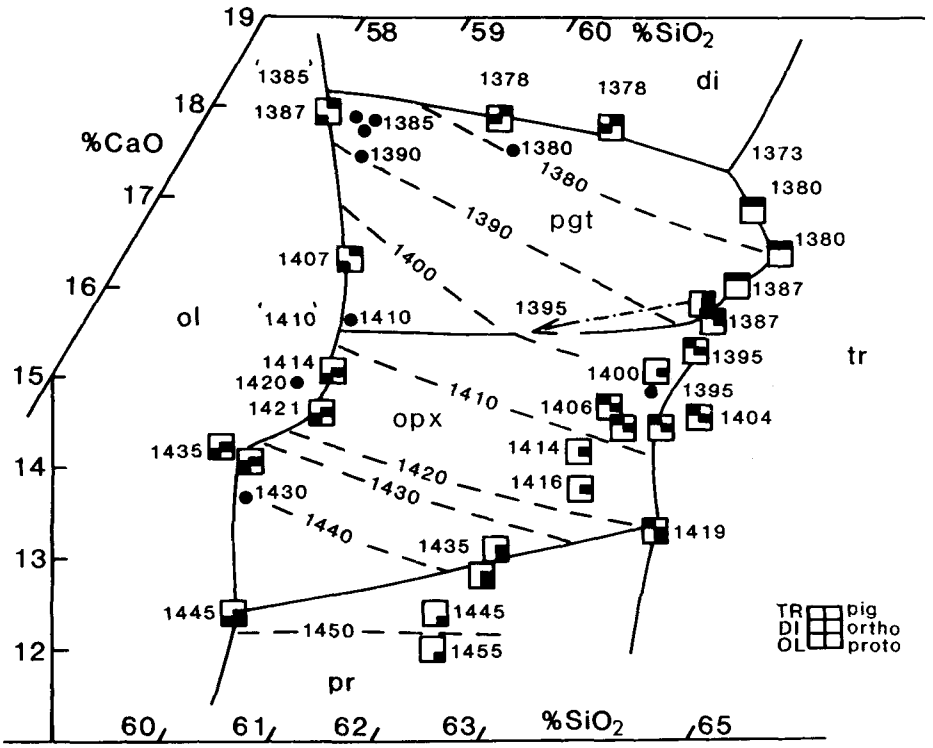

FIG. 1. Liquidus fields in the system CaO-MgO-SiO_2 based on glass analyses, all from Longhi and Boudreau (1980) but with suggested contours added. On the pigeonite-orthopyroxene boundary there is one problem run (at 1395 °C), the glass analysis of which seems to be out of place and the dashed-dot line is a suggested relocation. The symbols give the phases reported. Liquid is present in all runs. Also shown, as small filled circles, are analyses from Kushiro (1972). There are only minor conflicts between these data sets and these were fully discussed by Longhi and Boudreau (p. 567).

Orthopyroxene seems to be confined to CaO contents from 1.4 to 2.2 wt. % CaO.

These data can be used as a yardstick to compare other data. Kushiro's data for pigeonite in equilibrium with forsterite and liquid at 1400, 1390, and 1385 °C (fig. 4) give the locus *a'-b'* which agrees with *a-b* in respect of temperature and is only about 0.2 wt. % displaced in SiO_2 content. His data for pigeonite in equilibrium with diopside and liquid at 1380 and 1373 °C (open triangles) should be on the locus *b-d*. Two of Kushiro's analyses (open circles in fig. 4) were reinterpreted by Longhi and Boudreau as orthopyroxene and plot in the orthopyroxene range defined by the latter. Five analyses of protopyroxene are displaced by minor amounts of SiO_2 relative to those of Longhi and Boudreau. Indeed all Kushiro's analyses are of insignificantly lower SiO_2 content. Some new data from the experimental section of this paper are plotted in fig. 4. Details of the experimental method, and comments on the range of CaO contents of the crystals, and interpretations of this range in terms of an approach to equilibrium are all given in the next section. These new data for pigeonite compositions in equilibrium with forsterite and liquid give a curve, *a''-b''*, which is of scarcely significantly higher SiO_2 content than the two previous curves. At 1367 °C the sample was solid one-phase pigeonite.

Much of the data from figs. 1 to 4 is replotted in fig. 5 showing temperature versus CaO content of the crystals for assemblages with Ca-poor pyroxene, one other phase, and liquid present. Taken together, figs. 3 and 5 are offered as a more complete account of pyroxene compositions. For orthopyroxene the locus *e-f-g-h* is clearly defined by the data points for CaO *vs.* temperature in fig. 5 although the locus was confused for CaO versus SiO_2 in fig. 3. For pigeonite the locus *a-b-c-d* derives from Longhi and Boudreau but *a'-b'* from Kushiro and the analyses from Table I are broadly sympathetic (but see the comments in the experimental section about starting materials, run lengths, and product homogeneity). In the diagram

Table I Analyses from En_{90} Di_{10}

°C	SiO_2	MgO	CaO	Total
1500	59.50	39.23	0.39	99.13
	59.30	39.13	0.34	98.82
	58.99	39.25	0.31	98.58
1409	60.02	36.92	3.17	100.14
	59.83	35.72	3.97	99.53
	59.47	35.64	4.06	99.21
	59.76	36.48	3.48	99.74
	59.61	35.95	4.21	99.78
	59.55	36.34	3.82	99.74
	59.45	35.90	4.08	99.44
	59.51	36.08	3.88	99.47
	58.94	36.49	3.82	99.28
	58.95	36.32	3.89	99.18
1391	59.26	34.61	5.41	99.30
	58.76	34.39	5.75	98.93
	59.70	35.16	5.04	99.96
	59.29	35.46	4.63	99.40
	59.12	35.05	4.83	99.06
	58.91	35.06	4.84	98.88
	59.12	35.75	3.75	98.68
	59.30	35.83	3.78	98.96
	59.38	35.06	4.73	99.25
	59.51	35.57	4.17	99.30
	58.22	35.60	4.13	98.01
	58.97	36.28	4.20	99.49
	59.11	34.72	4.89	98.80
	58.93	34.37	5.61	98.98
	59.46	35.79	3.72	98.98
	58.94	36.77	3.82	99.54
	58.68	35.88	4.37	98.97
1367	59.52	35.61	4.02	99.21
	58.73	33.93	5.49	98.21
	59.32	33.82	6.17	99.42

The brackets link repeated analyses of the same crystal

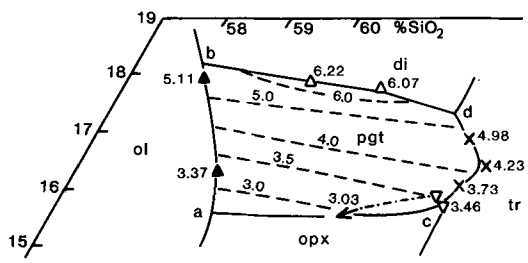

FIG. 2. The liquidus field of pigeonite from fig. 1, but the symbols have been simplified, and beside each glass analysis is a figure which is the CaO content of the coexisting crystalline pigeonite. From these values, contours of CaO content *in the crystals* are drawn across the *liquidus* surface.

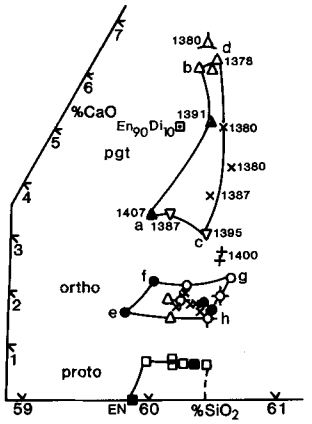

FIG. 3. Analyses of crystalline phases from Longhi and Boudreau (1980), but note that the SiO_2 axis is twice the scale of the CaO axis so that the real areas occupied by the crystalline solids are narrower. For scale, and reference, the composition $CaMg_{10}Si_{11}O_{33}$ is shown as $En_{90}Di_{10}$ ($M_9S_9+CMS_2$). If the enstatite formula is doubled to $Mg_2Si_2O_6$ this composition would be the molar composition $(M_2S_2)_{81.8}(CMS_2)_{18.2}$. It contains 5.01 wt.% CaO. In order to plot the analyses, which in general have totals from 98.5 to 100.5%, the analyses in this and subsequent figures were normalized to 100%. Data for pigeonite show several clear loci; *a–b* as filled triangles for pigeonite in equilibrium with forsterite and liquid; *c–d* as crosses for pigeonite in equilibrium with tridymite and liquid; *b–d* as open triangles for pigeonite in equilibrium with diopside (based on runs of one month duration at 1378 °C which contain pigeonite with less CaO than the pigeonite formed at 1380 °C for only one week). There is a locus *a–c*, confused in terms of temperature, for pigeonite in equilibrium with orthopyroxene, but this confusion results from the same 1395 °C run that was uncomfortable in fig. 1. Protopyroxene and orthopyroxene data can not be resolved in the same way. For example, for orthopyroxene the filled circles are in equilibrium with forsterite and the crosses are in equilibrium with tridymite and these two sets of symbols are intermingled. The loci based on *e–f–g–h* can be clearly resolved as shown later in fig. 5. The two plus signs are metastable orthopyroxenes, see text.

published by Longhi and Boudreau (their fig. 3) there is an area labelled orthoenstatite which despite appearances is not the same as *e–f–g–h* since their figure omits all data with tridymite present which here gives the locus *h–g*. Their caption implies subsolidus, whereas the locus *e–f–g–h* is all in equilibrium with liquid. (See further discussion in the section on subsolidus pyroxenes.)

Experimental results

The composition studied is shown as $En_{90}Di_{10}$ in figs. 3, 4, and 5. It was made up as a gel (Biggar

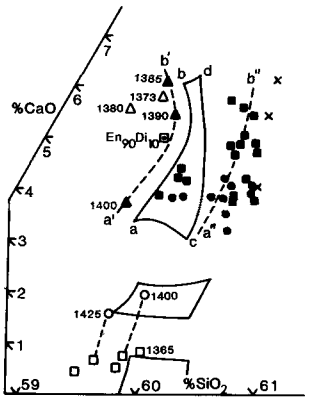

FIG. 4. Based on fig. 3 with additional data from Kushiro for pigeonite, as discussed in the text, giving the locus a'–b'. Data from Table I, filled circles at 1409 °C, filled squares at 1391 °C give the locus a''–b''. Data at 1367 °C are shown as crosses. Data for orthopyroxene and protopyroxene also come from Kushiro.

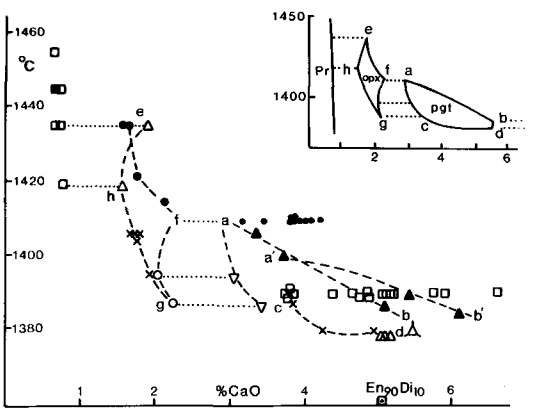

FIG. 5. CaO content of pyroxenes (data from Longhi and Boudreau, 1980) plotted against temperature for charges which also contained liquid and one other phase. The inset shows the smoothed conclusions. Symbols and loci of compositions are labelled *a* to *g*, as in fig. 3. Filled symbols with forsterite present, crosses with tridymite present, and coexisting pyroxenes linked by dotted tie-lines. Omitted from the figure are data for some charges which were orthopyroxene and liquid or pigeonite and liquid without other phases. Crystals from such charges should fall within the bounds defined and indeed they do or are very very close. Also added is the locus a'–b' from Kushiro (from fig. 4) and the data from Table I (small filled circles, 1409 °C and open squares, 1391 °C) which are in broad agreement with the a–b and a'–b' loci.

and O'Hara, 1969) and the experiments were actually done as long ago as 1968 at a time when neither orthopyroxene (Longhi and Boudreau, 1980) nor pigeonite (Kushiro, 1972) were known to exist on the join enstatite–diopside, and at a time when long runs (up to 1155 hours, Longhi and Boudreau) were not particularly common. The available experiments are 1500 °C for 65 h, 1409 °C for 3 days, 1391 °C for 4 days, 1367 °C for 21 days, 1304 °C for 22 days, 1265 °C for 18 days, and the original laboratory notes record all as pyroxene with occasional multiple twinning and a clinoenstatite X-ray diffraction pattern, so that originally all runs were interpreted as protopyroxene, inverted to clinopyroxene. It is now clear after optical re-examination that only the run at 1500 °C contains protopyroxene (Table I, 0.35 wt. % CaO) partially inverted to clinopyroxene with abundant, intricate, multiple twinning along irregular or *stepped* twin planes. The diffraction pattern shows small amounts of surviving protopyroxene. The other runs contain pigeonite (Table I, 3.2 to 5.8 wt. % CaO) with some twinning which in only a few crystals is repeated, to mimic the inversion twinning noted above, but the essential difference is that these repeated simple twins are along regular *unbroken* twin planes. There is no trace of protopyroxene in the diffraction patterns. The experiments at 1409 and 1391 °C contained some forsterite and liquid. The pigeonite crystals were up to 50 μm long. The experiment at 1367 °C was solid and although the pigeonite crystals were large, up to 30 μm, they were full of minute gas bubbles, not uncommon in recrystallized gels, and most microprobe analyses gave low totals, 85–95%. The experiments at 1304 and at 1265 °C gave 1 to 5 μm crystals identified as pigeonite by X-ray diffraction, but there were inhomogeneous patches in the products and despite the 18-day duration these are not at equilibrium.

Because most of the action takes place between 1373 and 1410 °C (fig. 1) and because both Longhi and Boudreau (1980) and Kushiro (1972) use the Geophysical Laboratory temperature scale with diopside melting at 1391.5 °C the temperatures of the above experiments have been quoted to conform.

Longhi and Boudreau comment on starting materials, run lengths, and homogeneity of products. They used glasses, devitrified at 1200 °C to produce submicroscopic intergrowths which during experiments of 48 to 1155 hours gave crystals of 10 to 100 μm of which orthoenstatite, pigeonite, and diopside were somewhat heterogeneous, pigeonite ranging from 5.46 to 7.68 wt. % CaO even after 1155 hours. Kushiro used a similar starting material and held his samples for 4 to 120 hours, and quotes ranges for CaO, for example 1.91 ± 0.21 for orthopyroxene. The present experi-

ments started from gels, known to crystallize initially to a 1 to 5 μm mass of crystals, which were then held for 3 to 21 days. Crystal inhomogeneity was investigated (Table I). At 1409 °C the analyses form a compact group (fig. 5) and within-crystal variation is not distinct from variation between crystals. At 1391 °C there is more variation, interpreted as variation (inhomogeneity or non-equilibrium) between crystals. The data in Table I show that repeated analyses of the same crystal generally gives very similar CaO contents ($\pm$0.2 wt. % CaO) but the next crystal is likely to have a different value such that the range spans from 3.7 to 5.7 wt. % CaO which is similar to that noted by Longhi and Boudreau from their starting material. At 1367 °C (solidus) very few analyses were acceptable and the three quoted in Table I spanned from 4.0 to 6.2 wt. % CaO and no conclusions about homogeneity should be made.

Table II. Analyses of alumina-bearing pyroxenes

A. Bulk Composition
SiO_2 58.1 Al_2O_3 2.5 (MgO 38.0 CaO 1.4)

°C	hr	SiO_2	Al_2O_3	MgO	CaO	Tot.
1500	65	59.02	0.16	38.97	0.11	98.25
1410	72	59.49	0.49	38.85	0.22	99.10
1410	72	59.78	0.60	39.03	0.29	99.73
1390	96	59.73	0.53	38.98	0.23	99.51
1390	96	59.71	0.52	38.92	0.23	99.42
1378	120	58.21	0.61	39.58	0.24	98.63
1339	48	59.92	0.85	38.77	0.36	99.94
		58.54	1.06	38.35	0.36	98.34

B. Compositions on the join enstatite alumina

1500	65	Average of 4	Al_2O_3	0.40%
1410	72	Average of 3	Al_2O_3	1.51%
1390	96	Average of 3	Al_2O_3	1.88%
1378	120	Average of 6	Al_2O_3	2.19%

Pyroxenes in the system CaO-MgO-Al_2O_3-SiO_2

All the published microprobe analyses of Ca-poor pyroxenes from this system and some new analyses from Table II, all at one bar, are plotted in fig. 6 and referenced in the caption without distinction as to the co-existing phases, or temperature, or to any identification given to the pyroxene by the

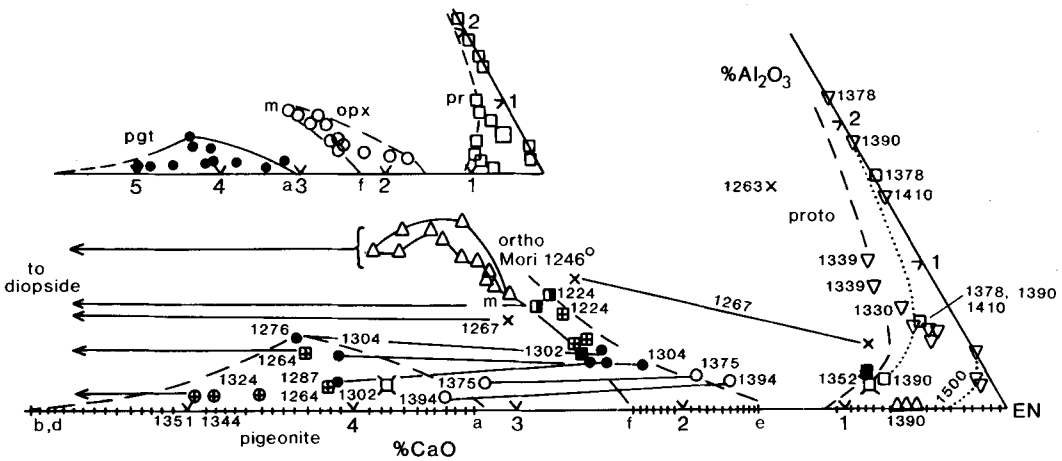

FIG. 6. Microprobe analyses of pyroxenes from experimental charges in the system CaO-MgO-Al_2O_3-SiO_2. Only the CaO and Al_2O_3 contents are plotted. An inset shows the simplified conclusion that the pyroxenes form three groups irrespective of the name given by the original authors. Coexisting pyroxenes are linked by tie lines. The alumina-free ranges are given by *e–f* and *a–b* (from fig. 5). Temperatures are those of the authors (mostly Geophysical Laboratory Scale, but Biggar and Clarke (1972) used IPTS-68 and data from Mori and Biggar (1981) are here converted to IPTS-68). Most data points are averages of several microprobe analyses, but individual analyses are shown from Mori (pers. comm.). Mori's data refer to the lowest temperature run shown in the figure and were probably the most difficult to analyse by microprobe, so that the range shown may reflect these difficulties. Accepting the analyses with least CaO and Al_2O_3, close to the point *m*, would be most consistent with the rest of the data. The charges analysed by Mori have been studied by X-ray diffraction which confirms that the pyroxene present is orthopyroxene. Some of the pyroxenes are distinguished by symbols. Circles are pyroxenes from Yang (1973), squares are from Biggar and Clarke (1972), crosses from Longhi (1978), triangles from Mori (pers. comm. and see Mori and Biggar, 1981) and inverted triangles are new data from Table II. If the above symbols are filled, forsterite was present, if the symbols are spiked tridymite was present, if the symbols have a plus sign inside them then diopside was a coexisting phase. Only two analyses, other than those of Mori, refer to pyroxenes coexisting with an aluminous phase, anorthite, and these are shown as half-filled squares. Protopyroxene accepts the most Al_2O_3 and will be in equilibrium with cordierite; orthopyroxene accepts less Al_2O_3; and pigeonite never enough alumina to be in equilibium with anorthite.

original authors. Fig. 6 shows the pyroxenes plotting in three groups, and in the several cases where two pyroxenes coexisted in an experiment tie-lines are shown between these groups. For the rest of this paper these chemical groupings are used to identify and name the pyroxene using the names shown in the figure. In almost all cases the original name given by the author is something different and if it is important the pyroxene in this paper will be named in the style orthopyroxene (was pigeonite) which is true for example of the two analyses shown as crosses in the orthopyroxene group at 1267 °C (at 2.7 and 2.2 wt. % CaO) which were called pigeonite by Longhi (1978). All three pyroxenes, in the past, have been very thoroughly confused, by almost all authors, but with hindsight, from fig. 6, we can perhaps see why. The worst offenders were perhaps Biggar and Clarke (1972) who called everything protopyroxene. In fig. 6 some of their pyroxenes are now seen to be pigeonite, some are orthopyroxene and some remain as protopyroxene. At least at the time that work was done (pre-1971) iron-free pigeonite at one bar (Kushiro, 1972) and iron-free orthopyroxene (Longhi and Boudreau, 1980) were not established. Virtually everything called protoenstatite by Yang (1973) is now accepted as orthopyroxene. Yang recognized both pyroxenes in short runs (1 day) at 1390 °C and commented that the one with polysynthetic twinning and cracks vanished in longer runs, and even stated that all his pyroxenes were twin free and crack free—which confirms that they are orthopyroxene as also detailed by Huebner (1980). Mori and Biggar (1981) followed Biggar and Clarke in calling everything protopyroxene. In connection with work done for this present paper the samples analysed by Mori (fig. 6), from experiments made by Biggar with gel starting materials, have now been shown by X-ray diffraction to be unambiguously orthopyroxene, establishing anorthite–forsterite–diopside–orthopyroxene as the subsolidus assemblage. In contrast, most previous publications (e.g. O'Hara and Schairer, 1963) record anorthite–fosterite–diopside–protopyroxene, from devitrified glass starting materials, which may make this another example of differences between gels and glasses (Biggar and O'Hara, 1969).

CaO and Al_2O_3 increase in the pyroxenes in fig. 6, in a manner broadly related to temperature decrease, but the diagram superimposes pyroxenes from many assemblages of coexisting phases and an orderly fall of temperature is not to be totally expected. Order comes from a study of the compositional ranges of pyroxenes when put in to perspective by sketching solid-solution polyhedra as in fig. 7. This figure replaces a polyhedron sketched by Biggar and Clarke (1972) at a time

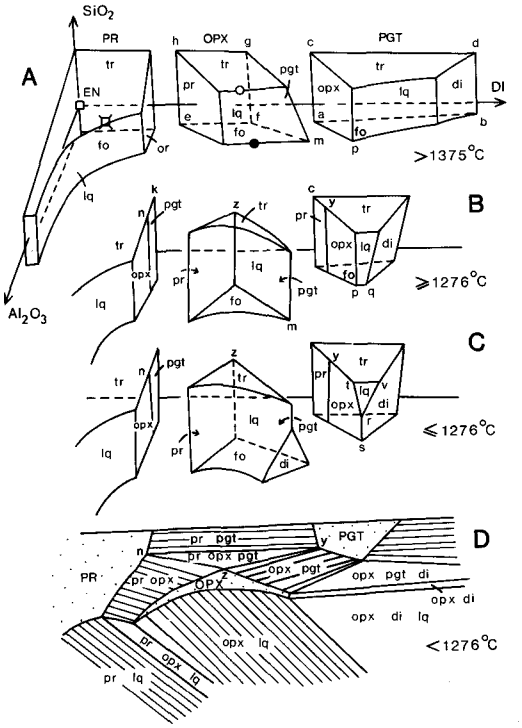

FIG. 7. Schematic solid-solution polyhedra for the three Ca-poor pyroxenes. This figure is based on and is a correction of fig. 2 of Biggar and Clarke (1972). Figure D is a sketch isothermal section through the middle of the polyhedra to demonstrate the geometry below 1276 °C with aluminous orthopyroxene stable.

when they believed that all the pyroxenes were protopyroxene. Each face of a polyhedron is the range of pyroxene compositions which are in equilibrium with one other phase (that phase is given by the abbreviations in the figure). Compositions which lie within the polyhedra are one-phase pyroxene, along edges two other phases coexist with the pyroxene, and at corners three other phases coexist. Fig. 7 accepts (from fig. 10) that alumina-free orthopyroxene reacts to protopyroxene and pigeonite at 1375 °C which would be expressed in fig. 7 by the condition that the face *e–f–g–h* has contracted to a line. At lower temperatures, for example fig. 7B, alumina-free protopyroxene, *k*, coexists with alumina-free pigeonite, *c*. Aluminous orthopyroxene remains stable to lower temperature as shown by the points *z* (in fig. 7B, C, and D) and coexists with aluminous protopyroxene, *n*, and aluminous pigeonite, *y*. Fig. 7B (> 1276 °C) and C (< 1276 °C) demonstrate the alumina-present univariant reaction $Fo + Pgt + Lq \rightleftharpoons Opx + Di$; expressed on the pigeonite polyhedron

as the edge *p–q* (where Fo and Lq meet) being replaced by the edge *r–s* (where Opx and Di meet); and on the orthopyroxene polyhedron by the apex *m* (where Fo, Pgt, Lq meet) being replaced by the face (Di). Pigeonite with liquid (the triangular face *r–t–v* in fig. 7C) is stable to lower temperatures, down to *w* (fig. 8) which represents the univariant point pigeonite–orthopyroxene–diopside–silica–liquid. Nothing is known about the decomposition of pigeonite in the solidus but as drawn in fig. 8, there is an inference that pigeonite-bearing solidus assemblages decompose to protoenstatite + diopside by about 1235 °C (see also fig. 10 for alumina-free pigeonite) where the pigeonite polyhedron must contract to a point, and vanish.

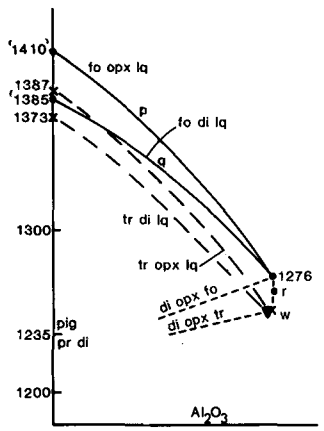

FIG. 8. Pigeonite is also present along all these loci, lettered to relate to previous diagrams. The Al_2O_3 axis is schematic and some of the curves represent loci of some of the apices of the pigeonite polyhedron of fig. 7. There are no data below 1276 °C to support the dashed lines.

Some of the confusion in fig. 6 arises from the differences in pyroxene composition depending on co-existing phases. As an example, some of the symbols from fig. 6 are sketched into fig. 7A mainly to illustrate that the orthopyroxene in equilibrium with forsterite, filled circle, and that in equilibrium with tridymite, open circle, will have different CaO, and Al_2O_3 (and SiO_2) contents at the same temperature, and will project at different places in fig. 6, despite synthesis at the same temperature.

Another reason for some of the confusion of the past can be ascribed to the universal use of temperature *vs.* CaO-content pseudo-binary diagrams. Only in a CaO *vs.* Al_2O_3 diagram such as fig. 6, are the pyroxenes separated into three groups. When CaO only is used (in effect projection from Al_2O_3) there is some overlap. For orthopyroxene, in particular, as temperature decreases CaO (and Al_2O_3) increase, for example from *f* to *m* (fig. 6), and it is this effect, that aluminous pyroxenes have greater CaO contents, that lead Longhi and Boudreau (1980) and Huebner (1980) to show a solvus with CaO increasing as temperature decreases, leading to bow-shaped fields which Longhi and Boudreau noted as 'not common in silicate systems'. A further discussion is given later but in effect they compared *f* with *m* (figs. 6 and 7). Likewise, in binary projections using only CaO, *m* (for an orthopyroxene) and *a* (for a pigeonite) overlap in CaO content.

Liquids in the system CaO–MgO–Al_2O_3–SiO_2

There are just sufficient microprobe analyses of glasses in the literature, equilibrated with some of the pyroxenes discussed in the last section (fig. 6), to be able to plot the liquidus fields, in forsterite projection with forsterite also present, of the four pyroxenes and this is done in fig. 9 along with some data from compositions studied by Yang (1973). The nature of the field boundaries and some crystallization paths can be determined. The field boundaries forsterite–protopyroxene–orthopyroxene and forsterite–orthopyroxene–pigeonite (fig. 9)

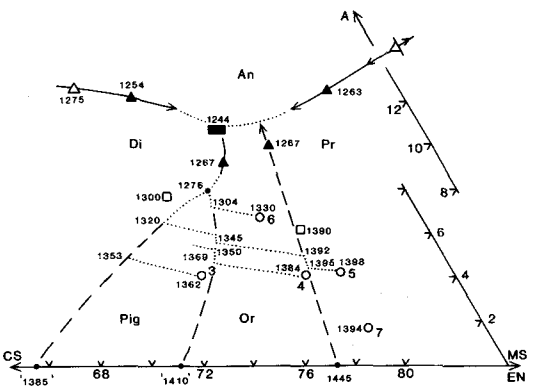

FIG. 9. Liquid compositions coexisting with forsterite and other phases, in the system CaO–MgO–Al_2O_3–SiO_2, projected from forsterite into the plane CS–MS–A shown as filled symbols. Triangles from Longhi (1978), squares from Mori and Biggar (1981) but note that their temperature of 1244 °C would become 1238 °C on the Geophysical Laboratory scale to which all other temperatures on this diagram belong. Data along the base come from fig. 1 and open triangles from O'Hara and Schairer (1963). The open symbols are bulk compositions of which something is known about their crystallization, numbered circles from Yang (1973), squares from O'Hara and Biggar (1969, p. 79). Dotted paths and temperatures are estimates used to describe crystallization paths in the text.

are both double resorption, clearly illustrated by the crystallization of Yang's sample No. 4, which crystallizes orthopyroxene (was proto) and forsterite at 1384 °C, picks up pigeonite at 1369 °C, has lost its forsterite by resorption at 1362 °C, and then lost by resorption its orthopyroxene by 1350 °C (this path is shown by dotted lines in fig. 9 although strictly speaking once it has lost its forsterite it should no longer be plotted in fig. 9 which is a forsterite projection).

Yang's composition 5 was only crystallized down to 1358 °C. Had its crystallization been continued it would have followed the dotted path crystallizing all four pyroxenes and resorbing three of them and then crystallizing for a second time one of them, as follows: protopyroxene (at 1398 °C), orthopyroxene at 1395 °C, protopyroxene resorbed by 1392 °C, pigeonite about 1345 °C, orthopyroxene resorbed by 1340 °C, diopside at 1320 °C, pigeonite resorbed at 1276 °C, and replaced by the second generation of orthopyroxene at 1276 °C. With such complexities around, perhaps some mistakes in the optical identification of pyroxenes in experimental charges can be forgiven.

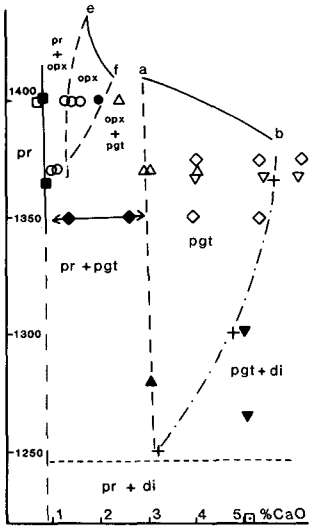

FIG. 10. Subsolidus data, strictly for compositions in CaO–MgO–SiO_2 at one bar. Symbols and data described in the text.

Subsolidus pyroxenes, $MgSiO_3$–$CaMgSi_2O_6$

The subtle differences in pyroxene composition between each apex of the solid solution polyhedra (fig. 7), for example, that *f* for an alumina-free orthopyroxene is not the same as *m*, means that as temperature changes *f* will generate a locus *F* and *m* a locus *M*. The locus *M* may terminate with a reaction of alumina-bearing orthopyroxene to other phases but the locus *F* will continue to some other temperature at which a similar (but alumina-free) reaction may occur. All recent diagrams for the join enstatite–diopside have mingled data relevant to *F* and *M*, drawn one locus, and of course had problems at terminations. The points 1276 and W (fig. 8) are an example of a similar effect, for pigeonite.

The bow-shaped fields of Longhi and Boudreau (1980) and of Huebner (1980) in general derive from data appropriate to *f* at higher temperature, and *m* at lower temperature. These authors all appreciated these deficiencies without stating them so directly. Huebner said that his diagram might be correct for the iron-free system but was more likely to be correct when iron and alumina are present to stabilize orthopyroxene, and Longhi and Boudreau said that sub-solidus phase relationships still defy precise representation. The data are re-assessed in fig. 10. Since the forsterite liquidus volume lies above the join En–Di the solidus for orthopyroxene will be *e*–*f*, and for pigeonite will be *a*–*b* (from fig. 5). The diopside limb of the pigeonite solvus is moderately well determined starting from point *b* (fig. 3) from Longhi and Boudreau at 1378 °C and continuing with the X-ray diffraction data of Boyd and Schairer (1964) at 1365, 1300, and 1250 °C shown as crosses. Other subsolidus syntheses of pigeonite are inverted triangles at 1367 °C (Table I) and triangles at 1370 °C from Jenner and Green (1983) at 1370 °C. Jenner and Green also re-ran their 1370 °C pigeonite at 1280 °C and demonstrated no change (shown as a filled triangle) although a direct synthesis attempted at the same time at 1280 °C retained metastable phases. The gel studied in this paper was similar. When held at 1304 °C and at 1265 °C (shown as filled inverted triangles) it gave pigeonite but with traces of unreacted silica, suggesting that pigeonite is formed down to these temperatures but that the subsolidus reactions are sluggish. Diopside can also be presumed to be present in these runs. Warner and Luth (1974) synthesized pigeonite at 1375 °C and at 1350 °C (open diamonds) and found the assemblage protopyroxene + pigeonite at 1350 °C (filled diamonds). All these data allow construction of the boundaries of a pigeonite field, and only one datum for pigeonite, at 1400 °C from Jenner and Green (1983) with 2·0 to 2·6 wt. % CaO, plotted at 2·3 % CaO, is not easily accommodated. It has generally been accepted that the pigeonite field terminates at about 1240 °C and protopyroxene and diopside become stable.

Orthopyroxene synthesis has been achieved by

Kushiro (1972) in one sample at 1400 °C (filled circle) and the following direct quote from Longhi and Boudreau reinterprets some other data, 'careful examination of enstatite-rich run products at 1365 °C (Boyd and Schairer, 1964) and at 1350 °C (Warner and Luth, 1974) failed to reveal any orthoenstatite. Boyd and Schairer did, however, report orthoenstatite ('rhombic enstatite') at 1395 °C, which *they* interpreted as a quench product'. The above suggests that at 1395 °C orthopyroxene was stable (and not quench) and at 1365 °C it did not form. After Longhi and Boudreau proposed this interpretation Jenner and Green (1983) have recorded orthopyroxene at 1400 °C (open circles at 1.21, 1.40, and 1.54% CaO) and protopyroxene (open square). Taken with other protopyroxene data from Kushiro (filled squares) the protopyroxene solvus can be drawn. A controversy now arises from Jenner and Green's data at 1370 °C, *j* in fig. 10, for orthopyroxenes with 0.94 and 0.97% CaO. On the basis of fig. 6 these would be protopyroxene, and if one accepts this reinterpretation then Jenner and Green did not synthesize orthopyroxene at 1370 °C whilst they did at 1400 °C, entirely in sympathy with the above Longhi and Boudreau interpretation. This reinterpretation is used to postulate (uphold) the termination of orthopyroxene at 1375 ± 10 °C. There are no other dry, flux-free, data and fig. 10 is thus the extent of our knowledge of the subsolidus of En–Di, *sensu stricto*.

Revised Schreinemaker's curves

For the system CaO–MgO–SiO_2 the previously published Schreinemaker's analysis with the greatest information about the data used is that of Mori and Green (1975). Warner (1975) shows virtually the same diagram. In both these papers the hydrothermal data of Boyd and Schairer (1964) obtained at 1 kbar for the reaction opx ⇌ pr + di [PGT] are extrapolated to 1100 °C at one bar. Jenner and Green (1983) point out that the diagram of Longhi and Boudreau (1980), which accepts the same extrapolation, and simultaneously proposes pr + pgt ⇌ opx [DI] at 1375 °C is inconsistent with Schreinemaker's rules. Since fig. 10 also accepts the reaction at 1375 °C, one needs to consider an alternative Schreinemaker's analysis (proposed in fig. 11) which accepts these high temperature, dry, data for [DI] at 1375 °C, and refuses to extrapolate 1 kbar data of Boyd and Schairer to one bar. Data for the other two curves are not in dispute; the reaction opx + di ⇌ pgt [PR] is bracketed between 1325 °C and 1375 °C at 5 kbar and is known at 17.5 kbar at 1450 °C as reviewed by Warner (1975, p. 1417); and the reaction pr + di ⇌ pgt [OPX] is at about 1240 °C at one bar (Warner, p. 1416, and in fig. 10).

Some comments on data for the curve [PGT], essentially the work of Boyd and Schairer are appropriate. Since dry samples will not equilibrate, these hydrothermal experiments have to be used, and there remain the reservations that at these lower temperatures equilibrium may not have been reached or that water could have had an effect on the placement of the curve. Boyd and Schairer went to enormous lengths to try and prove (reverse) the equilibrium at 1, 500, and 1000 bars, at temperatures up to 1150 °C, but their text and tables are full of examples of the persistence of metastable phases. Some direct quotes are 'hydrothermal runs in the range 1000–1100 °C usually yield mixtures of all forms of Mg-rich pyroxene' (p. 293); 'equilibrium relations . . . are not well established' (p. 293); and 'synthesis from a glass does not define a stability field' (p. 300). On balance their data support opx + di at 1 kbar and other data in fig. 11 confirm this at 2 and 5 kbar. This is accepted in fig. 11 by placing the curve [PGT] about 1 kbar but not

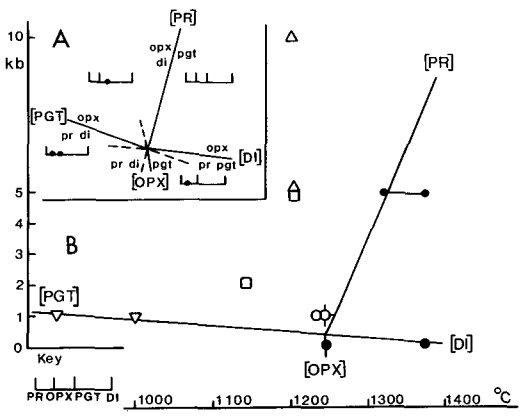

FIG. 11. A, inset to show the Schreinemaker's analysis, and to identify the reactions. The real data in B require that [PGT] and [DI] are nearly colinear. A selection of data points crystallizing opx + di ± vapour is shown by open symbols; triangles from Mori and Green (1975); inverted triangles from Boyd and Schairer (1964); circles from Warner (1975); and squares from Warner and Luth (1974). In addition, Warner (p. 1417) records the assemblage from 900–1300 °C at 10, 5, and 2 kbar although his published points (Warner and Luth, 1974) only demonstrate 1200 °C at 5 kbar and 1150 °C at 2 kbar. At 1 kbar Warner quotes results at 1235 °C and 1240 °C which he admits are confusing (p. 1416). In fig. 11 the circle at 1235 °C has the correct assemblages, Pr + En or En + Di, for the field in which it is shown plotted, and the spiked circle for Di + Pr is the only datum in fig. 11 which is not consistent with the Schreinemaker's curves.

allowing it to come as low as one bar, and not allowing the alternative that the reaction [PGT] is curved in PT space. In summary, the high temperature (1375 °C) fix on the curve [DI] is given preference to extrapolation of the low-temperature (and hydrothermal) data for [PGT].

REFERENCES

Biggar, G. M., and Clarke, D. B. (1972) *Lithos*, **5**, 125–9.
—— and O'Hara, M. J. (1969) *Mineral. Mag.* **37**, 198–205.
Boyd, F. R., and Schairer, J. F. (1964) *J. Petrol.* **5**, 275–309.
Huebner, J. S. (1980) *Reviews in Mineralogy* Min. Soc. Am. **7**, 213–88.
Jenner, G. A., and Green, D. H. (1983) *Mineral. Mag.* **47**, 153–60.
Kushiro, I. (1972) *Am. Mineral.* **57**, 1260–71.
Longhi, J. (1978) *Proc. 9th Lunar Sci. Conf.* Suppl. Geochim. Cosmochim. Acta, 285–306.
—— and Boudreau, A. E. (1980) *Am. Mineral.* **65**, 563–73.
Mori, T., and Biggar, G. M. (1981). *Prog. Exptl. Petrol.* 5th Rept. N.E.R.C. London, 144–7.
—— and Green, D. H. (1975) *Earth Planet. Sci. Lett.* **26**, 277–86.
O'Hara, M. J. and Biggar, G. M. (1969) *Prog. Exptl. Petrol.* 1st Rept. 79–81.
—— and Schairer, J. F. (1963) *Carnegie Inst. Washington Yearb.* **62**, 107–15.
Warner, R. D. (1975) *Geochim. Cosmochim. Acta*, **39**, 1413–21.
—— and Luth, W. C. (1974) *Am. Mineral.* **59**, 98–109.
Yang, H-Y. (1973) *Am. J. Sci.* **273**, 488–97.

[*Manuscript received 23 September 1983; revised 24 August 1984*]